

# Full spectroscopic model and trihybrid experimental-perturbative-variational line list for NH

Armando N. Perri<sup>ID</sup> and Laura K. McKemmish<sup>ID</sup>\*

*School of Chemistry, University of New South Wales, 2052, Sydney, Australia*

24 May 2024

## ABSTRACT

Imidogen (NH) is a reactive molecule whose presence in astrochemical environments is of interest due to its role in the formation of nitrogen-containing molecules and as a potential probe of nitrogen abundance. Spectroscopic NH monitoring is useful for Earth-based combustion and photolysis processes of ammonia and other nitrogen-containing species. NH is also relevant to ultracold molecular physics and plasma studies. To enable these diverse applications, high-quality molecular spectroscopic data is required. Here, a new line list with significant advantages over existing data is presented. Most notably, this line list models isotopologue spectroscopy and forbidden transitions (important for NH visible absorption), alongside some overall improvements to accuracy and completeness. This approach takes advantage of existing experimental data (from a previous MARVEL compilation) and perturbative line lists together with new MRCI *ab initio* electronic data. These are used to produce a novel variational spectroscopic model and trihybrid line list for the main  $^{14}\text{N}^1\text{H}$  isotopologue, as well as isotopologue-extrapolated hybrid line lists for the  $^{14}\text{N}^2\text{H}$ ,  $^{15}\text{N}^1\text{H}$  and  $^{15}\text{N}^2\text{H}$  isotopologues. The new  $^{14}\text{N}^1\text{H}$  ExoMol-style trihybrid line list, κNIGHT, comprises 4,076 energy levels (1,078 experimental) and 327,014 transitions up to  $47,500\text{ cm}^{-1}$  (211 nm) between five low-lying electronic states (X  $^3\Sigma^-$ , a  $^1\Delta$ , b  $^1\Sigma^+$ , A  $^3\Pi$  and c  $^1\Pi$ ). For most anticipated applications aside from far-IR studies, this line list will be of sufficient quality; any improvements should focus on the b  $^1\Sigma^+$  energies, and the a  $^1\Delta$  – A  $^3\Pi$  and b  $^1\Sigma^+$  – A  $^3\Pi$  spin-orbit couplings.

**Key words:** molecular data - ISM: molecules - stars: general - astronomical data bases: miscellaneous - astrochemistry - opacity

## 1 INTRODUCTION

Imidogen (NH) is a reactive free radical diatomic molecule that is likely the simplest nitrogen-containing compound in the universe. Its spectroscopic properties, however, make it quite challenging to observe in astronomical environments. Nevertheless, NH has been observed in a wide variety of systems, as recently discussed in Civiš et al. (2023). Briefly, as a non-exhaustive list of observational studies, NH has been detected in the atmosphere of the Sun (Babcock 1945; Grevesse et al. 1990; Civiš et al. 2023), the interstellar medium (Meyer & Roth 1991; Crawford & Williams 1997; Cernicharo et al. 2000; Weselak et al. 2009; Persson, C. M. et al. 2010, 2012), comets (Swings et al. 1941) and cool stars (Snedden 1973;

Lambert et al. 1984; Smith & Lambert 1986; Aoki & Tsuji 1997). Many of these studies use NH as a proxy to quantify nitrogen abundance in a way that is independent of other elemental abundances (assuming that hydrogen is in excess).

As a reactive free radical, NH plays an important chemical role in the astrochemical production of molecules, with current chemical models incorporating NH as a reactant or intermediate, for example, in the formation of  $\text{N}_2$  (Bhasi et al. 2015), ammonia (Mann & Williams 1984) and even the DNA nucleotide base cytosine (Gupta et al. 2013). Based on the observed abundance of NH in interstellar space, the formation of NH is generally accepted to occur on dust grains (Mann & Williams 1984; Wagenblast et al. 1993), although radiative association of N and H atoms could contribute in low-dust environments (Szabó & Gustafsson 2019).

NH is also a prominent reactive intermediate in many

\* E-mail: l.mckemmish@unsw.edu.au

non-astronomical contexts and thus spectroscopic monitoring of NH can provide insights into reaction pathways in varied environments. For example, NH is monitored to understand the chemistry of ammonia photolysis (an important sink in Earth’s atmosphere) (Hikida et al. 1988) and various plasma systems (Pflieger et al. 2017; Hamdan et al. 2018; Harilal et al. 2018). The chemistry of ammonia and other nitrogen-containing compounds during combustion, understood through NH spectroscopy, thus holds significant contemporary relevance (Glarborg et al. 2018; Brackmann et al. 2018; Lamoureux et al. 2019; zhi Jin et al. 2022; Mashruk et al. 2023). Further, ammonia is emerging as a promising alternative fuel source. It is imperative, however, to prevent incomplete combustion in order to avoid the undesirable generation of NO<sub>x</sub> pollutants.

At the other end of the temperature scale, NH is of interest for experimental investigations within ultracold molecular physics, with various efforts proposed or demonstrated for cooling. Specifically, NH has already been cooled with buffer gases into a magnetic trap (Campbell et al. 2007), decelerated using the Stark effect (van de Meerakker et al. 2006) and Zeeman effect (Plomp et al. 2019). NH has also been proposed as a candidate for laser cooling (Li & Bian 2021; Yan et al. 2021) due to the similarities in the A <sup>3</sup>Π and X <sup>3</sup>Σ<sup>-</sup> potential energy surfaces leading to a near-diagonal A <sup>3</sup>Π – X <sup>3</sup>Σ<sup>-</sup> transition with a Frank-Condon factor of 0.999472 (Liu et al. 2020), which minimises loss mechanisms in the laser cooling process.

As alluded to above, despite its simplicity, the position and strength of the spectral bands of NH can make it a challenging molecule to detect astrophysically. The visible region only has weak spectral features from forbidden transitions or vibrationally excited initial states with low Boltzmann population. In the literature, NH is most commonly detected astronomically through its strong ultraviolet bands at approximately 335 nm, but ground-based observations suffer from significant atmospheric molecular absorption in this window (Weselak et al. 2009). Since NH is such a light molecule, the pure rotational bands move into the far infrared spectral region ( $\approx 1$  THz) accessible by few telescopes; the first observation of this band (according to the thorough literature review of McGuire (2022)) was in 2000 by Cernicharo et al. (2000) using Infrared Space Observatory (in operation 1995 – 1998). The mid-infrared vibrational transitions are allowed and span a considerable spectral range for hot stars, but ground-based observations do need to be cautious of telluric absorption. New and emerging opportunities with the next generation in space-based infrared telescopes starting with JWST mean that the detection of NH in this region is becoming easier.

In order to understand and observe molecules in space, astronomers rely on line lists, that is, the set of molecular energies and transition intensities between these energy levels; this data is a crucial input to models of astronomical objects and necessary to interpret observationally spectroscopically-resolved data. For NH, Bernath and co-workers have constructed the MoLLIST line list using the traditional approach (based on an effective Hamiltonian treatment), with X <sup>3</sup>Σ<sup>-</sup> rovibrational and rotational transitions considered in Brooke et al. (2014, 2015) and A <sup>3</sup>Π – X <sup>3</sup>Σ<sup>-</sup> rovibronic transitions modelled in Fernando et al. (2018). These data

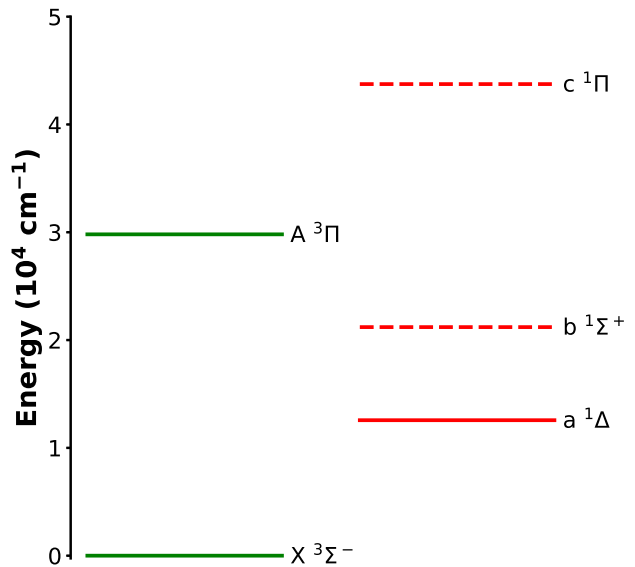


**Figure 1.** The five lowest electronic states of NH with term energies  $T_e$  from Huber & Herzberg (1979). The solid lines indicate electronic states fit to experimental data in this work.

were made available in the conventional ExoMol format in Villanueva et al. (2018).

Despite this, there are a number of opportunities to improve these spectral data, which have been acted upon herein to produce kNIGHT, the best line list currently available for <sup>14</sup>N<sup>1</sup>H and its isotopologues across the UV to mid-IR regions (studies of the far-IR region should instead utilise the Splatalogue database (Remijan et al. 2007), which includes hyperfine-resolved rotational data from JPL (Pickett et al. 1998) and CDMS (Endres et al. 2016)). Importantly, the trihybrid approach used in this paper combines experimental (MARVEL) data, perturbative (MoLLIST) data and novel variational data from a fitted spectroscopic model (potential energy, dipole moment and coupling curves) to produce a line list that has both high accuracy of strong line positions and high completeness (for opacity calculations and radiative transfer modelling). This approach has been previously used in the line list construction of CN (Syme & McKemmish 2021) and ZrO (Perri et al. 2023) in accordance with the ExoMol project (Tennyson & Yurchenko 2012; Tennyson et al. 2020). It should be noted that accurate variational calculations for diatomic molecules using global coupled channels (*e.g.* Amiot et al. (1999); Letelier & Senent (2006); Rey & Tyuterev (2007); Le Roy (2017)) have proved successful for many decades.

Specifically, the new kNIGHT line list improves the existing MoLLIST data in three ways. Firstly, it includes additional singlet electronic states and spin-orbit coupling between states, which allow for the spin-forbidden b <sup>1</sup>Σ<sup>+</sup> – X <sup>3</sup>Σ<sup>-</sup> and a <sup>1</sup>Δ – X <sup>3</sup>Σ<sup>-</sup> visible transitions (Yarkony 1989) to be modelled. These forbidden transitions are actually the dominant absorption source over almost all of the visible spectral region. Second, it incorporates the recently compiled comprehensive and self-consistent MARVEL energy levels for <sup>14</sup>N<sup>1</sup>H, which include almost all experimental assigned transitions (see Darby-Lewis et al. (2019) for

details) in order to increase the quality of the predicted transition frequencies. The nature of this combined experimental analysis has allowed for unprecedented accuracy of spectral line positions with reliable quantum number assignment (J.-M. Flaud & Maillard 1976; Furtenbacher et al. 2007). Finally, the variational approach based on a fitted spectroscopic model employed here trivially allows the generation of isotopologue spectra that are challenging to obtain using traditional perturbative approaches.

The new κNIGHT line list could also be of significant interest to the ultracold molecular physics community, where these data could be used to model the laser cooling mechanism in fine detail to quantify all loss mechanisms including intersystem crossing. The effects of the  $a^1\Delta - A^3\Pi$  and  $b^1\Sigma^+ - A^3\Pi$  spin-orbit couplings quantified in this work may be particularly useful, especially given the *ab initio* spin-orbit coupling curves that are calculated. The limitations of the κNIGHT line list are explicitly discussed and future potential areas for improvement are identified.

This article is structured as follows; an overview of the literature experimental, perturbative and *ab initio* spectroscopic data are presented in Section 2. *Ab initio* data are presented in this section. In Section 3, the spectroscopic model for the main  $^{14}\text{N}^1\text{H}$  isotopologue is constructed based on *ab initio* curves fitted to experimental data. In Section 4, variational line lists are generated for the  $^{14}\text{N}^1\text{H}$ ,  $^{14}\text{N}^2\text{H}$ ,  $^{15}\text{N}^1\text{H}$  and  $^{15}\text{N}^2\text{H}$  isotopologues, as well as tri-hybrid and isotopologue-extrapolated hybrid line lists. In Section 5, partition functions and cross sections are analysed. The accuracy of the total  $^{14}\text{N}^1\text{H}$  cross section is considered in the context of astronomical observations from both JWST and similar space-based telescopes, as well as for high-resolution cross-correlation methodologies using ground-based telescopes.

## 2 $^{14}\text{N}^1\text{H}$ SPECTROSCOPIC DATA

The rovibronic spectroscopy of NH is characterised primarily by the five electronic states in Figure 1 (Owono Owono et al. 2007; Song et al. 2016). The ground  $1\sigma^2 2\sigma^2 3\sigma^2 1\pi^2$  electronic configuration gives the ground  $X^3\Sigma^-$  electronic state, as well as the low-lying excited  $a^1\Delta$  and  $b^1\Sigma^+$  electronic states. Excitation into the  $1\sigma^2 2\sigma^2 3\sigma^1 1\pi^3$  electronic configuration produces the  $A^3\Pi$  and  $c^1\Pi$  electronic states. The  $A^3\Pi - X^3\Sigma^-$  rovibronic system dominates the spectrum, however, the spin-forbidden  $a^1\Delta - X^3\Sigma^-$  and  $b^1\Sigma^+ - X^3\Sigma^-$  may be observed over the  $X^3\Sigma^-$  rovibrational system in the visible region due to  $a^1\Delta - A^3\Pi$  and  $b^1\Sigma^+ - A^3\Pi$  spin-orbit couplings. As the Boltzmann population of the  $a^1\Delta$  electronic state is negligible even at high temperatures, transitions between singlet states are not important to the spectroscopy of thermally-equilibrated NH.

### 2.1 Experimental data

In the literature, the main  $^{14}\text{N}^1\text{H}$  isotopologue has been investigated through many experimental spectroscopic studies. This was recently reviewed and collated in Darby-Lewis et al. (2019), which obtained assigned rovibronic transitions from eighteen publications (Bernath & Amano 1982; Ramsay & Sarre

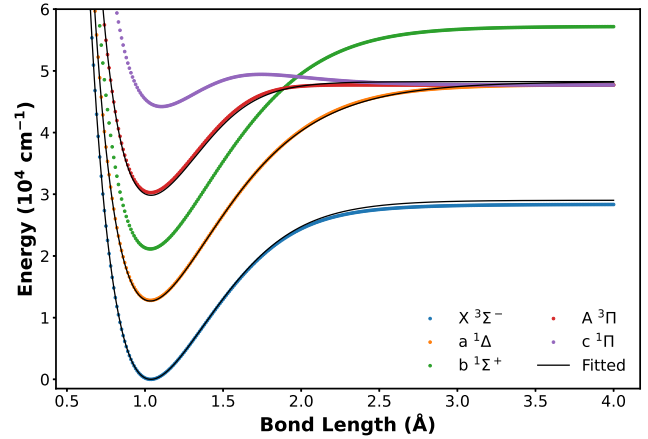


**Figure 2.** The potential energy curves of the five lowest electronic states of  $^{14}\text{N}^1\text{H}$ . The coloured dots show the *ab initio* data calculated in this work. The solid black lines illustrate the final curves fit for the  $X^3\Sigma^-$ ,  $a^1\Delta$  and  $A^3\Pi$  electronic states, which were modelled using an extended Morse oscillator curve fit to the MARVEL experimental data.

1982; van den Heuvel et al. 1982; Hall et al. 1985; Boudjaadar et al. 1986; Brazier et al. 1986; Leopold et al. 1986; Ram & Bernath 1986; Ubachs et al. 1986; Hack & Mill 1990; Geller et al. 1991; Klaus et al. 1997; Ram et al. 1999; van de Meerakker et al. 2003; Flores-Mijangos et al. 2004; Lewen et al. 2004; Robinson et al. 2007; Ram & Bernath 2010) derived from both laboratory measurements and astronomical spectra. Using the MARVEL (Furtenbacher et al. 2007) algorithm, the 3,002 rovibronic transitions validated were inverted to give a set of empirical energies for rovibronic states belonging to the  $X^3\Sigma^-$ ,  $A^3\Pi$ ,  $a^1\Delta$  and  $c^1\Pi$  electronic states. These energies form one self-consistent spectroscopic network containing 1,058 rovibronic states. Apart from unresolved  $\Lambda$ -doubling in the  $a^1\Delta$  electronic state, all fine structure is characterised using Hund’s coupling case (b). The  $b^1\Sigma^+$  electronic state data were found to be sparse and thus not included in the study.

### 2.2 Perturbative line lists

Beyond the experimental data collated by Darby-Lewis et al. (2019), there exists only perturbative line lists for NH in the literature. The perturbative (or traditional) methodology relies on an effective Hamiltonian, where experimental data are fit to polynomial expressions through the optimisation of spectroscopic parameters for each electronic state. This approach allows for the prediction of unobserved transitions with *ab initio* dipole moment curves. This provides a natural extension to experimental data, where the associated line lists interpolate experimental energies to high accuracy. Due to corrections obtained through perturbation theory, however, perturbative line lists typically extrapolate poorly, especially to higher vibrational levels. For this reason, they are often incomplete as they are limited by experimental data.

Perturbative line lists for  $^{14}\text{N}^1\text{H}$  were generated by both Brooke et al. (2014, 2015) and Fernando et al. (2018). The former line list contains  $X^3\Sigma^-$  rovibrational and rotational

transitions with fine structure characterised using Hund’s coupling case (b). The Einstein A coefficients were derived from an *ab initio* diagonal dipole moment curve calculated using the MRCI/aug-cc-pV6Z model chemistry. These transition intensities were revised in [Brooke et al. \(2015\)](#) using an improved method of converting the transition dipole matrix elements from Hund’s coupling case (b) to (a) as required by PGOPHER ([Western 2017](#)). The latter line list specifies A  $^3\Pi - X^3\Sigma^-$  rovibronic transitions with fine structure characterised using Hund’s coupling case (b). The off-diagonal dipole moment curve was calculated using the MRCI/aug-cc-pwCV5Z model chemistry. These two perturbative line lists were compiled into the conventional ExoMol format by [Villanueva et al. \(2018\)](#) to form the previous most comprehensive line list for  $^{14}\text{N}^1\text{H}$  across the UV to mid-IR regions.

There is no variational line list currently available for NH in the literature that has been constructed through numerical solution of the nuclear Schrödinger equation. This prevents reliable extrapolation to unobserved rovibrational states.

### 2.3 *Ab initio* data

*Ab initio* spectroscopic data have been calculated for many electronic states of NH to varying accuracy. The most comprehensive studies were performed by [Owono Owono et al. \(2007\)](#) and [Song et al. \(2016\)](#), which both consider many low-lying and high-lying Rydberg electronic states. Similar calculations were performed with fewer electronic states in other publications ([Li & Bian 2021](#); [Brooke et al. 2014, 2015](#); [Fernando et al. 2018](#)). Despite this previous body of work, raw output data are generally not provided or important details, such as off-diagonal (transition) dipole moment curves are missing, which emphasises the importance of data availability as discussed in [McKemmish \(2021\)](#). Therefore, new *ab initio* calculations were necessary for this study.

In this work, *ab initio* calculations were performed in Molpro 2020.1 ([Werner et al. 2020](#)) using the icMRCI-SD/aug-cc-pwCV5Z model chemistry with reference orbitals obtained from SA-CASSCF calculations. Using the  $(a_1, b_1, b_2, a_2)$  irreducible representation of the  $C_{2v}$  point group,  $(3, 1, 1, 0)$  active orbitals from (N:  $2s, 2p$ ; H:  $1s$ ) and  $(1, 0, 0, 0)$  closed orbitals from (N:  $1s$ ) were selected. These orbitals were optimised for the  $X^3\Sigma^-$ , A  $^3\Pi$ , a  $^1\Delta$ , b  $^1\Sigma^+$  and c  $^1\Pi$  electronic states with equal weighting. These *ab initio* calculations utilise the same model chemistry as [Brooke et al. \(2014, 2015\)](#) and [Fernando et al. \(2018\)](#), but were expanded to include the singlet a  $^1\Delta$ , b  $^1\Sigma^+$  and c  $^1\Pi$  electronic states.

## 3 $^{14}\text{N}^1\text{H}$ SPECTROSCOPIC MODEL

There is currently no available spectroscopic model (*i.e.* a set of self-consistent potential energy, coupling and dipole moment curves used in the variational model of a molecule, see [McKemmish \(2021\)](#) for details) fit to experimental data for  $^{14}\text{N}^1\text{H}$  in the literature. The absence of this model hinders physically reasonable extrapolation to new unobserved transitions.

Here, the  $^{14}\text{N}^1\text{H}$  spectroscopic model is assembled for

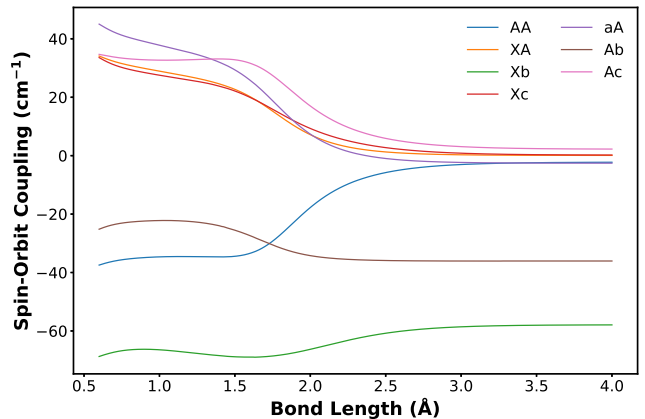


**Figure 3.** The  $^{14}\text{N}^1\text{H}$  *ab initio* spin-orbit coupling curves calculated in this work.

the five  $X^3\Sigma^-$ , a  $^1\Delta$ , b  $^1\Sigma^+$ , A  $^3\Pi$  and c  $^1\Pi$  electronic states in a Duo ([Yurchenko et al. 2016](#)) .model input file.

### 3.1 Energy spectroscopic model

The  $^{14}\text{N}^1\text{H}$  energy spectroscopic model comprises the potential energy curve of each electronic state, as well as the coupling and correction curves between these states. Firstly, the potential energy curves for the five electronic states considered are shown in Figure 2. The b  $^1\Sigma^+$  and c  $^1\Pi$  curves were taken from the *ab initio* data in Section 2.3. The  $X^3\Sigma^-$ , a  $^1\Delta$  and A  $^3\Pi$  states were modelled using an extended Morse oscillator potential given by

$$V(R) = T_e + D_e \left[ 1 - \exp \left( \sum_{i=0}^N b_i \left( \frac{R^4 - R_e^4}{R^4 + R_e^4} \right)^i (R_e - R) \right) \right]^2 \quad (1)$$

where  $T_e$  is the term energy,  $D_e$  is the dissociation energy,  $R_e$  is the equilibrium bond length and  $\{b_i\}$  are vibrational fitting parameters. The number of these fitting parameters differs on the left and right of the equilibrium bond length as specified by the parameters  $N_L$  and  $N_R$  in the .model input file, respectively. The dissociation asymptote  $A_e = T_e + D_e$  was set to  $29,030 \text{ cm}^{-1}$  ([Ram & Bernath 2010](#)) for the  $X^3\Sigma^-$  electronic state and  $48,256 \text{ cm}^{-1}$  ([Brazier et al. 1986](#)) for the A  $^3\Pi$  and a  $^1\Delta$  electronic states in accordance with [Fernando et al. \(2018\)](#).

The  $X^3\Sigma^-$ , a  $^1\Delta$  and A  $^3\Pi$  potential energy curves were fit to 1,053 unique MARVEL experimental energies ([Darby-Lewis et al. 2019](#)), where the inverse square of each MARVEL uncertainty was applied as the weighting factor in the fitting procedure. The degenerate MARVEL rovibronic states with unresolved  $\Lambda$ -doubling were duplicated with opposite parity for completeness. The *ab initio* potential energy curves from Section 2.3 were used to further confine the fit. The fitted parameters for the  $X^3\Sigma^-$ , a  $^1\Delta$  and A  $^3\Pi$  potential energy curves are provided in Table 1.

Additionally, all spin-orbit ( $A_{SO}$ ), spin-spin ( $\lambda_{SS}$ ), spin-rotation ( $\gamma_{SR}$ ),  $\Lambda$ -doubling ( $\lambda_{opq}$ ,  $\lambda_{p2q}$  and  $\lambda_q$ ), angular momentum ( $L_+$ ) and Born-Oppenheimer breakdown ( $BO_{rot}$ ) interactions relevant to the  $X^3\Sigma^-$ , a  $^1\Delta$  and A  $^3\Pi$  electronic states were considered in this energy spectroscopic model. Specifically, the Born-Oppenheimer breakdown correction allows for a position-dependent variation of the rotational mass ([Le Roy & Huang 2002](#); [Brady et al. 2023](#)), which is treated here for  $^{14}\text{N}^1\text{H}$  only. This has shown to be

**Table 1.** The fitted variational parameters of the potential energy and diagonal coupling curves for the  $X^3\Sigma^-$ ,  $a^1\Delta$  and  $A^3\Pi$  electronic states. Apart from the dimensionless parameters  $N_L$  and  $N_R$ , all parameters are rounded to five significant figures in units of  $\text{\AA}$  for  $R_e$ ,  $\text{\AA}^{-i}$  for the  $b_i$  vibrational parameters and  $\text{cm}^{-1}$  otherwise. The exact parameters employed can be found in the .model file.

Parameter	$X^3\Sigma^-$	$a^1\Delta$	$A^3\Pi$
$T_e$	+0.0000E+00	+1.2697E+04	+2.9828E+04
$R_e$	+1.0374E+00	+1.0340E+00	+1.0385E+00
$A_e$	+2.9030E+04	+4.8256E+04	+4.8256E+04
$N_L$	2	2	2
$N_R$	6	4	4
$b_0$	+2.2744E+00	+2.0838E+00	+2.8059E+00
$b_1$	+5.1944E-02	-3.7475E-02	+3.7475E-01
$b_2$	+1.2097E-01	+8.9429E-02	+2.7966E-01
$b_3$	-1.1310E-01	-1.5469E-01	-4.6666E-02
$b_4$	+1.0407E+00	+3.1844E-01	+1.3859E+00
$b_5$	-1.8662E+00	-	-
$b_6$	+1.5602E+00	-	-
$\lambda_{SS}, B_0$	+5.3994E-01	-	-1.7225E-01
$\lambda_{SS}, B_1$	+6.3032E-01	-	-3.3004E-01
$BO_{\text{rot}}, B_0$	+2.3019E-03	-4.9957E-04	+2.2394E-03
$\gamma_{SR}, B_0$	+2.4946E-03	-	-7.7438E-04
$\gamma_{SR}, B_1$	+1.0706E-02	-	+2.6870E-02
$\lambda_{p2q}, B_0$	-	-	+1.3716E+00
$\lambda_{opq}, B_0$	-	-	-4.9803E-03
$\lambda_q, B_0$	-	-	-4.0109E-05

**Table 2.** A statistical summary of the  $^{14}\text{N}^1\text{H}$  absolute energy residuals grouped by electronic state for each vibrational state  $v$  in the MARVEL analysis. The number of rovibronic states ( $n$ ), as well as the root mean square error (RMSE), mean absolute error (MAE) and maximum residual in units of  $\text{cm}^{-1}$ , are presented for each vibronic level.

State	$v$	$n$	RMSE	MAE	Maximum
$X^3\Sigma^-$	0	105	1.641E-01	1.111E-01	4.533E-01
	1	103	2.232E-01	1.841E-01	3.787E-01
	2	97	1.773E-01	1.465E-01	3.052E-01
	3	86	2.784E-02	1.751E-02	1.107E-01
	4	64	8.715E-02	8.244E-02	1.833E-01
	5	51	6.191E-02	5.551E-02	1.019E-01
$a^1\Delta$	6	36	1.753E-01	1.332E-01	4.415E-01
	0	36	1.339E-02	6.319E-03	5.873E-02
	1	38	1.819E-02	1.056E-02	7.775E-02
	2	24	4.362E-02	3.916E-02	7.690E-02
$A^3\Pi$	3	12	4.901E-02	4.203E-02	8.717E-02
	0	181	6.496E-02	4.455E-02	3.012E-01
	1	139	4.513E-02	2.955E-02	1.642E-01
$c^1\Pi$	2	82	3.394E-02	2.946E-02	7.599E-02
	0	22	9.001E-01	6.370E-01	2.220E+00
	1	2	1.205E+01	1.205E+01	1.206E+01

important for hydrides with large rotational constants, such as NH (Melosso et al. 2019), HF (Le Roy 1999) and MgH (Henderson et al. 2013), in order to account for electronic centrifugal distortion. The spin-orbit and angular momenta curves obtained from the *ab initio* calculations in Section 2 were inserted into the model without fitting to any functional form. The *ab initio* spin-orbit curves are shown in Figure 3. The remaining curves are purely empirical in nature and were fit to the MARVEL experimental data using

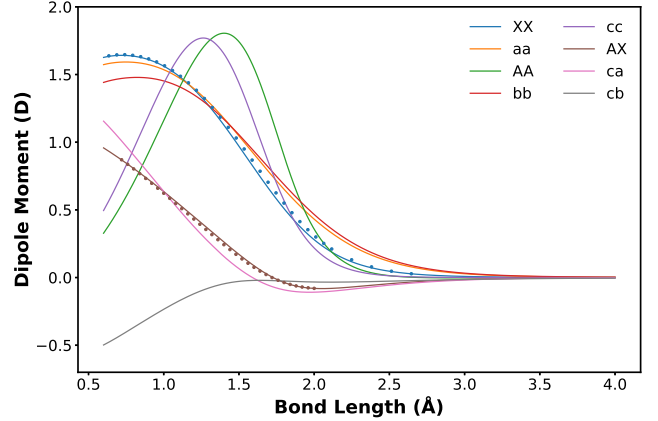


**Figure 4.** The  $^{14}\text{N}^1\text{H}$  *ab initio* dipole moment curves calculated in this work. The coloured dots indicate values calculated by Brooke et. al. (2014, 2015) and Fernando et. al. (2018), where a phase difference has been assumed for the  $A^3\Pi - X^3\Sigma^-$  dipole moment curve.

the damped polynomial given by

$$F(R) = \sum_{i=0}^N B_i \left[ (R - R_e) e^{-(R-R_e)^2} \right]^i \left( 1 - \frac{R^2 - R_e^2}{R^2 + R_e^2} \right) \quad (2)$$

These empirical interactions improve the overall quality of the fit, but decay to zero for large bond lengths in order to ensure good extrapolation. The diagonal coupling parameters are provided in Table 1.

Ultimately, the fitted energy spectroscopic model constructed herein can accurately reproduce the MARVEL experimental energies for all electronic states. This is shown by the absolute energy residuals summarised statistically in Table 2, which were calculated as the absolute difference between the MARVEL experimental and variational energies.

In Table 3, the  $X^3\Sigma^-$  and  $A^3\Pi$  equilibrium spectroscopic parameters from this  $^{14}\text{N}^1\text{H}$  model are compared to selected literature studies. There is a general agreement across all sources.

### 3.2 Intensity spectroscopic model

The  $^{14}\text{N}^1\text{H}$  intensity spectroscopic model contains only *ab initio* dipole moment curves as is standard practice. These were inserted into the .model file without fitting to a functional form, where all interpolation was performed by Duo using natural splines. The intensity spectroscopic model includes all diagonal (permanent) and off-diagonal (transition) dipole moment curves shown in Figure 4. This figure also includes values calculated by Brooke et al. (2014, 2015) and Fernando et al. (2018) for the  $X^3\Sigma^- - X^3\Sigma^-$  and  $A^3\Pi - X^3\Sigma^-$  curves, respectively. Their values are in close agreement with the new data; this is unsurprising given the electronic simplicity of NH and indicates that both dipole moment *ab initio* data are of high quality.

**Table 3.** The  $^{14}\text{N}^1\text{H}$  equilibrium spectroscopic parameters from selected sources reported without error estimates in units of  $\text{\AA}$  for  $R_e$  and  $\text{cm}^{-1}$  otherwise.

State	Parameter	$\kappa\text{NIGHT}$	<i>Ab initio</i>	H & H (1979)	Brazier et al. (1986)	Song et al. (2016)
X $^3\Sigma^-$	$A_e$	29,030	28,341	27,987	29,030	29,153.70
	$\omega_e$	3,281.8	3,279.1	3,282.27	3,282.220	3,292.07
	$\omega_e x_e$	78.099	–	78.35	78.513	86.66
	$R_e$	1.0374	1.0369	1.03621	–	1.0375
	$B_e$	16.668	16.678	16.6993	16.667704	16.74
	$D_e$ ( $10^{-4}$ )	17.175	17.257	17.097	–	–
	$\alpha_e$	0.64354	0.66548	0.649	0.649670	0.632
	$T_e$	29,828	30,262	29,807.4	29,790.5	29,794.77
	$A_e$	48,256	47,715	–	48,256	48,186.62
	$\omega_e$	3,225.8	3,238.7	3,231.2	3,231.70	3,263.32
A $^3\Pi$	$\omega_e x_e$	96.24	–	98.6	98.48	97.73
	$R_e$	1.0385	1.0369	1.03698	–	1.0368
	$B_e$	16.668	16.678	16.675	16.681963	16.69
	$D_e$ ( $10^{-4}$ )	17.666	17.690	17.800	–	–
	$\alpha_e$	0.70933	0.72193	0.7454	0.712880	0.711

## 4 NH LINE LIST CONSTRUCTION

### 4.1 Methodology overview

The line list construction approach of Syme & McKemmish (2021) and Perri et al. (2023) is followed herein for NH, where the MARVEL experimental, MoLLIST perturbative and Duo variational energies are collated into a trihybrid line list. This methodology exploits the advantages of each methodology to produce  $\kappa\text{NIGHT}$ , the most accurate and comprehensive line list for NH currently available.

Specifically, high accuracy is attributed to the high-resolution experimental MARVEL energies from Darby-Lewis et al. (2019) complemented by a small number of interpolated perturbative (effective Hamiltonian) energies from Brooke et al. (2014, 2015); Fernando et al. (2018). High completeness arises from a new spectroscopic model (fitted to experimental data) constructed in the previous section that yields a variational line list. The experimental, perturbative and variational energies are combined to generate a novel trihybrid line list for  $^{14}\text{N}^1\text{H}$ , named  $\kappa\text{NIGHT}$ . Isotopologue energies for  $^{14}\text{N}^2\text{H}$ ,  $^{15}\text{N}^1\text{H}$  and  $^{15}\text{N}^2\text{H}$  are predicted from this main line list using standard techniques, where  $^{14}\text{N}$ ,  $^{15}\text{N}$ ,  $^1\text{H}$  and  $^2\text{H}$  have an isotopic abundance of 99.63, 0.37, 99.985 and 0.015 per cent, respectively (Brown & Carrington 2003).

In accordance with ExoMol line lists conventions, a trihybrid line list is prepared by updating the energies of the variational .states file. The trihybrid methodology prioritises the experimental energies due to their superior accuracy and reliable uncertainties. These replace the variational energies wherever possible with subsequent interpolation by the perturbative energies. The final trihybrid .states file includes the methodology and variational energy of each state, where the abbreviations Ma, EH and Ca represent the experimental (MARVEL), perturbative (effective Hamiltonian) and variational (calculated) methodologies, respectively.

The  $^{14}\text{N}^1\text{H}$  variational line list is output directly from Duo using the energy and intensity spectroscopic model detailed in Section 3. The quantum numbers are given in terms of Hund’s coupling case (a), which were converted to case (b). The  $^{14}\text{N}^1\text{H}$  trihybrid line list was created by replacing the variational energies with MARVEL experimen-

tal energies (Darby-Lewis et al. 2019) where available, followed by interpolation with MoLLIST perturbative energies (Brooke et al. 2014, 2015; Fernando et al. 2018) to cover any missing experimental data. The variational energies of the *ab initio*  $c^1\Pi$  electronic state were shifted here to match the MARVEL analysis for the lowest energy level. These energy transformations were performed using an external Python script by grouping equivalent rovibronic states from each source by their electronic state, parity,  $v$ ,  $J$  and  $N$  quantum numbers.

For all other isotopologues, a variational line list can be constructed trivially by changing the nuclear mass(es) in the main spectroscopic model. Following Polyansky et al. (2017), the accuracy of this line list can be improved by applying an isotopologue extrapolation term that shifts each energy based on the difference between the variational and trihybrid line lists of the main  $^{14}\text{N}^1\text{H}$  isotopologue as

$$\tilde{E}_{\text{IE}}^{\text{iso}} = \tilde{E}_{\text{Ca}}^{\text{iso}} + \left( \tilde{E}_{\text{tri}}^{\text{main}} - \tilde{E}_{\text{Ca}}^{\text{main}} \right) \quad (3)$$

where  $\tilde{E}_{\text{Ca}}^{\text{main}}$  is the calculated variational energy of the main isotopologue,  $\tilde{E}_{\text{tri}}^{\text{main}}$  is its trihybrid energy,  $\tilde{E}_{\text{Ca}}^{\text{iso}}$  is the calculated variational energy of a given isotopologue and  $\tilde{E}_{\text{IE}}^{\text{iso}}$  is its isotopologue-extrapolated energy. In other words, it is assumed that the energy residuals between the hybridised and variational line lists are constant for all isotopologues.

NH is a light molecule that is best described using Hund’s coupling case (b), and previous line lists have thus assigned quantum numbers under this regime. As Duo diagonalises the total rovibronic Hamiltonian using case (a) basis functions, however, the conversion to case (b) was a significant challenge faced in this work. For the X  $^3\Sigma^-$  electronic state, a simple empirical relationship was determined between the  $N$  quantum number and the  $\Omega = \Sigma$  quantum number assigned by Duo. For the A  $^3\Pi$  electronic state, an empirical relationship could not be determined that was consistent for all energy. The  $N$  quantum number was thus assigned in an external Python script using based on energy orderings with comparison to existing line lists. For the singlet electronic states, there are no complications as  $N = J$  in the absence of electronic spin, where  $J$  is well-defined and always conserved. Despite these issues, it is important to note that Duo solves the Schrödinger equation using a com-

**Table 4.** An extract from the  $^{14}\text{N}^1\text{H}$  .states file. The total file is available at [www.exomol.com](http://www.exomol.com) and in the supplementary material.

$n$	$E$	$g_{\text{tot}}$	$J$	unc	$\tau$	$g$	$p_{+/-}$	$p_{e/f}$	State	$v$	$\Lambda$	$N$	$F$	Source	$\tilde{E}_{\text{Ca}}$
38	29829.555340	6	0	1.1500E-03	3.5430E-07	0.0000E+00	-	f	A(3PI)	0	-1	1	3	Ma	29829.507210
39	32862.788560	6	0	3.7136E-02	3.9583E-07	0.0000E+00	-	f	A(3PI)	1	-1	1	3	EH	32862.755435
40	35698.984598	6	0	7.5995E-02	4.4710E-07	0.0000E+00	-	f	A(3PI)	2	-1	1	3	Ca	35698.984598
41	38325.477243	6	0	6.0248E-01	5.1244E-07	0.0000E+00	-	f	A(3PI)	3	-1	1	3	Ca	38325.477243

**Table 5.** The column descriptors of the NH .states files. Here,  $\hat{L}$  is the electronic orbital angular momentum.

Column	Symbol	Descriptor
1	$n$	State Index
2	$\tilde{E}$	Energy (in $\text{cm}^{-1}$ )
3	$g_{\text{tot}}$	Total Degeneracy
4	$J$	Total Angular Momentum
5	unc	Uncertainty (in $\text{cm}^{-1}$ )
6	$\tau$	Lifetime (in s)
7	$g$	Landé $g$ -Factor
8	$p_{+/-}$	Total Parity
9	$p_{e/f}$	Rotationless Parity
10	State	Electronic State
11	$v$	Vibrational State
12	$\Lambda$	$\hat{L}$ Projection Along Internuclear Axis
13	$N$	Rotational Angular Momentum
14	$F$	Fine Structure Counting Number
15	Source	State Source (Ma, EH or Ca)
16	$\tilde{E}_{\text{Ca}}$	Variational (Calculated) Energy (in $\text{cm}^{-1}$ )

**Table 6.** An extract from the  $^{14}\text{N}^1\text{H}$  .trans file. The total file is available at [www.exomol.com](http://www.exomol.com) and in the supplementary material.

$f$	$i$	$A_{fi}$
83	1	4.5597E-02
84	1	3.2919E+00
85	1	8.7746E+00
86	1	9.2748E-02

**Table 7.** The column descriptors of the NH .trans files.

Column	Symbol	Descriptor
1	$f$	Final State Index
2	$i$	Initial State Index
3	$A_{fi}$	Einstein A Coefficient (in $\text{s}^{-1}$ )

plete basis set and thus the energy of the quantum state is accurate despite the use of Hund’s coupling case (a) in the calculation; indeed, the quantum numbers themselves (aside from  $J$  and parity) are simply labels assigned based on dominant contribution to describe the wavefunction and have no influence on the final cross sections.

## 4.2 Line list overview

The κNIGHT trihybrid .states file contains 4,076 rovibronic states with 1,078 (1,023 unique) experimental states, 76 perturbative states and 2,922 variational states. These were calculated up to  $47,500 \text{ cm}^{-1}$ , which is just below the dissociation asymptote  $A_e$  of the  $a^1\Delta$ ,  $b^1\Sigma^+$ ,  $A^3\Pi$  and  $c^1\Pi$  electronic states. A vibrational basis set up to  $v = 60$  was used for each electronic state with rotational states calculated to  $J = 60$ . An extract of the final .states files is shown Table 4 with associated column descriptors in Table 5.

The κNIGHT trihybrid .trans file contains 327,014 transitions. All transitions were calculated up to  $47,500 \text{ cm}^{-1}$ .

**Table 8.** A statistical summary of the absolute frequency residuals between κNIGHT and Melosso et. al. (2019) grouped by isotopologue and transition type. The root mean square error (RMSE), mean absolute error (MAE) and maximum residual are presented in units of  $\text{cm}^{-1}$ .

Isotopologue	Type	RMSE	MAE	Maximum
$^{14}\text{N}^1\text{H}$	Rotational	2.910E-04	5.000E-04	1.275E-03
$^{14}\text{N}^1\text{H}$	Infrared	2.336E-03	3.618E-03	1.856E-02
$^{14}\text{N}^2\text{H}$	Rotational	4.498E-03	5.197E-03	9.616E-03
$^{14}\text{N}^2\text{H}$	Infrared	5.357E-01	5.550E-01	8.312E-01
$^{15}\text{N}^1\text{H}$	Rotational	6.986E-04	7.497E-04	1.175E-03
$^{15}\text{N}^1\text{H}$	Infrared	5.385E-04	8.674E-04	2.191E-03
$^{15}\text{N}^2\text{H}$	Rotational	4.081E-03	4.592E-03	8.361E-03

An extract of the final .trans files is shown Table 6 with associated column descriptors in Table 7.

Additionally, isotopologue-extrapolated hybrid line lists were prepared for  $^{14}\text{N}^2\text{H}$ ,  $^{15}\text{N}^1\text{H}$  and  $^{15}\text{N}^2\text{H}$  using the technique in Section 4.1. In Table 8, experimental X  $^3\Sigma^-$  rovibrational transition frequencies for all four isotopologues are compared statistically to the κNIGHT line list. These experimental transition frequencies were collated by Melosso et al. (2019) from twelve sources and divided into rotational and infrared transitions with all hyperfine structure averaged over. There is excellent agreement for all isotopologues, where the largest residuals are observed for the  $^{14}\text{N}^2\text{H}$  infrared transitions. It should be noted that these isotopologue data are sparse with a maximum upper  $v = 6$ ,  $J = 27$  for the  $^{14}\text{N}^2\text{H}$  infrared transitions and  $v = 0$ ,  $J = 8$  for the  $^{15}\text{N}^1\text{H}$  infrared transitions.

## 4.3 Uncertainties

The uncertainties assigned to the experimental, perturbative and variational energies were all evaluated differently. For the main  $^{14}\text{N}^1\text{H}$  isotopologue, the experimental uncertainties were obtained directly from the MARVEL analysis. The perturbative uncertainties were averaged from the experimental uncertainties with the same vibrational and rotational quantum numbers, where the experimental and perturbative energies are known to have similar accuracy when interpolating. The variational uncertainties were approximated using the energy residuals in Table 2. For energies within a vibrational state in the MARVEL analysis, the uncertainty is given as the largest energy residual with the same vibrational quantum number. For energies within a vibrational state unknown by the MARVEL analysis, the uncertainty is given as the twice the largest energy residual in the same electronic state. The  $b^1\Sigma^+$  uncertainties were set to  $100 \text{ cm}^{-1}$ .

For the other three isotopologues, all X  $^3\Sigma^-$ ,  $a^1\Delta$ ,  $A^3\Pi$  and  $c^1\Pi$  uncertainties were increased by an order of magnitude to account for errors arising from the isotopologue-extrapolation technique. The  $b^1\Sigma^+$  uncertainties were kept at  $100 \text{ cm}^{-1}$ .

## 5 NH LINE LIST ANALYSIS

ExoCross (Yurchenko et al. 2018) was used to generate partition functions and cross sections for all four NH isotopologues studied here.

### 5.1 Partition functions

The partition functions  $Q(T)$  were calculated using

$$Q(T) = \sum_n g_n^{\text{ns}} (2J_n + 1) e^{-c_2 \tilde{E}_n / T} \quad (4)$$

where  $g_n^{\text{ns}}$  is the nuclear spin statistical weight factor,  $J$  is the total angular momentum excluding nuclear spin,  $c_2 = hc/k_B$  (in cm K),  $\tilde{E}$  is the energy term value (in  $\text{cm}^{-1}$ ) and  $T$  is temperature (in K).

In Table 9, the four partition functions are evaluated at selected temperatures. For  $^{14}\text{N}^1\text{H}$ , the partition function is compared to values calculated by MoLLIST and Barklem & Collet (2016). There is strong agreement between the κNIGHT data and Barklem & Collet (2016), even at 5,000 K, thus strongly corroborating both data sets. There is also strong agreement with the MoLLIST data, where the differences at 5,000 K arise due to the inclusion of higher vibrational bands from the variational calculations. Therefore, the κNIGHT trihybrid line list provides only marginal improvements to the partition functions and is primarily included for line list completeness and ease of access.

### 5.2 Cross sections

Here, cross sections are presented for the main  $^{14}\text{N}^1\text{H}$  isotopologue only. The absorption cross sections in Figures 5, 6 and 7 were simulated using a Gaussian lineshape with a half-width at half-maximum of  $20 \text{ cm}^{-1}$  (artificially large to aid visibility; NH will not exhibit significant Doppler broadening in its common astronomical environments).

In Figure 5, the total  $^{14}\text{N}^1\text{H}$  absorption cross section at 2,000 K is decomposed into its primary transition bands for  $0 - 47,500 \text{ cm}^{-1}$ . The spectrum possesses many intense transitions in all spectral regions. The ultraviolet region is the most prominent, where the  $\text{A } ^3\Pi - \text{X } ^3\Sigma^-$  transitions dominate. The spin-forbidden  $\text{a } ^1\Delta - \text{X } ^3\Sigma^-$  and  $\text{b } ^1\Sigma^+ - \text{X } ^3\Sigma^-$  systems are observable over the  $\text{X } ^3\Sigma^-$  rovibrational system in the visible region.

In Figure 6, the total  $^{14}\text{N}^1\text{H}$  absorption cross section at 2,000 K is generated using three line lists. The black, blue and orange cross sections indicate transitions provided by the trihybrid, MARVEL experimental (with variational intensities) and MoLLIST perturbative line lists, respectively. As expected, the trihybrid line list produces the most comprehensive cross section due to its inclusion of the variational transition intensities calculated in this work. The MARVEL analysis offers good coverage of the  $\text{A } ^3\Pi - \text{X } ^3\Sigma^-$  and  $\text{a } ^1\Delta - \text{X } ^3\Sigma^-$  rovibronic transitions, as well as the  $\text{X } ^3\Sigma^-$  rovibrational system. The MoLLIST analysis agrees well with the trihybrid cross section for the main vibrational bands of the  $\text{A } ^3\Pi - \text{X } ^3\Sigma^-$  manifold. The  $\text{a } ^1\Delta - \text{X } ^3\Sigma^-$  and  $\text{b } ^1\Sigma^+ - \text{X } ^3\Sigma^-$  rovibronic transitions are not included in the MoLLIST line lists.

In Figure 7, the total  $^{14}\text{N}^1\text{H}$  absorption cross section

is simulated at several temperatures. The weaker bands in the cross section increase in intensity and all bands become broader with some shape changes with increasing temperature.

### 5.3 High-resolution considerations

In order to assess the suitability of a line list for use in the HRCC detection of a molecule, it is critical to know the accuracy with which line positions are known. The accuracy of a transition frequency depends on the source of the energies of its upper and lower state. If both the upper and lower state energies are known from MARVEL data (with typically low uncertainties), then its frequency can be assumed to be known to high accuracy. Conversely, if one or both of the energies are calculated from the Duo variational spectroscopic model, then the frequency will have much higher uncertainty; it is assumed here that it is insufficiently accurate for HRCC studies. The effective Hamiltonian perturbative data can be neglected from this discussion due to the low number of energies in the κNIGHT line list.

Again, in Figure 6, the cross section of the full κNIGHT trihybrid line list (assumed to be near complete based on partition function considerations and the inclusion of all low-lying electronic states) is compared with the cross section predicted solely by MARVEL data (assumed to be highly accurate). In spectral regions where the two curves overlap, it should be understood that the transition frequency of the strong line is predicted to experimental (MARVEL) accuracy. In this case, Figure 6 shows that the κNIGHT trihybrid line list has sufficient accuracy to be suitable for HRCC primarily between  $22,500 - 35,000 \text{ cm}^{-1}$  ( $280 - 444 \text{ nm}$ ) and below  $15,000 \text{ cm}^{-1}$  (above  $667 \text{ nm}$ ) at 2,000 K. Despite this, many spectral lines are relatively weak or in spectral regions that are difficult to observe, such as the strong UV lines near  $30,000 \text{ cm}^{-1}$  ( $333 \text{ nm}$ ). The most easily observed transitions are probably the N – H fundamental stretch vibrational band near  $3,300 \text{ cm}^{-1}$  ( $3.03 \mu\text{m}$ ). These conclusions are based on the 2,000 K cross section, but are readily generated at different temperatures using ExoCross and can be examined at higher resolutions to ensure suitability for a desired application.

A useful complementary perspective on high-resolution completeness is obtained from Figure 8. This plot is read by looking at vertical slices to visualise the source of upper and lower state energies for transitions above that intensity. For example, the vertical slice at  $10^{-20} \text{ cm molecule}^{-1}$  shows that about 60 per cent of all transitions with intensity of  $10^{-20} \text{ cm molecule}^{-1}$  have both upper and lower energies from the high-resolution MARVEL data; however, this still leaves about 40 per cent of lines at 2,000 K whose positions are not sufficiently accurate for HRCC.

Despite the high accuracy of the data for high-resolution cross-correlation, it must be noted that for NH specifically, most of the strong bands are in challenging spectral regions for ground-based observations and thus the high-resolution cross-correlation techniques are likely to face considerable challenges. Space-based observations are thus highly preferable for detecting NH.

**Table 9.** The partition functions for NH as a function of temperature  $T$  (in K) from different sources. The main  $^{14}\text{N}^1\text{H}$  isotopologue compares the data produced in this work to values calculated by MoLLIST and Barklem & Collet (2016).

$T$ (K)	$^{14}\text{N}^1\text{H}$	$^{14}\text{N}^1\text{H}$	$^{14}\text{N}^1\text{H}$	$^{14}\text{N}^2\text{H}$	$^{15}\text{N}^1\text{H}$	$^{15}\text{N}^2\text{H}$
	κNIGHT	MoLLIST	B & C (2016)	κNIGHT	κNIGHT	κNIGHT
0	6.00000E+00	6.00000E+00	6.00000E+00	9.00000E+00	4.00000E+00	6.00000E+00
1	1.80000E+01	1.80000E+01	1.80000E+01	2.70000E+01	1.20000E+01	1.80000E+01
10	1.84915E+01	1.84915E+01	1.84904E+01	3.35570E+01	1.23345E+01	2.24658E+01
100	8.29087E+01	8.29090E+01	8.29164E+01	2.23111E+02	5.54978E+01	1.49931E+02
300	2.36350E+02	2.36350E+02	2.36370E+02	6.51909E+02	1.58246E+02	4.38188E+02
500	3.90556E+02	3.90557E+02	3.90595E+02	1.08377E+03	2.61507E+02	7.28531E+02
800	6.25183E+02	6.25184E+02	–	1.75922E+03	4.18635E+02	1.18289E+03
1,000	7.87584E+02	7.87585E+02	7.87722E+02	2.24860E+03	5.27422E+02	1.51233E+03
1,500	1.23471E+03	1.23471E+03	1.23510E+03	3.67378E+03	8.27054E+02	2.47240E+03
2,000	1.76222E+03	1.76209E+03	1.76315E+03	5.43911E+03	1.18069E+03	3.66229E+03
3,000	3.11676E+03	3.11089E+03	3.12054E+03	1.01364E+04	2.08903E+03	6.82969E+03
5,000	7.36897E+03	7.13095E+03	7.40652E+03	2.53046E+04	4.94084E+03	1.70616E+04

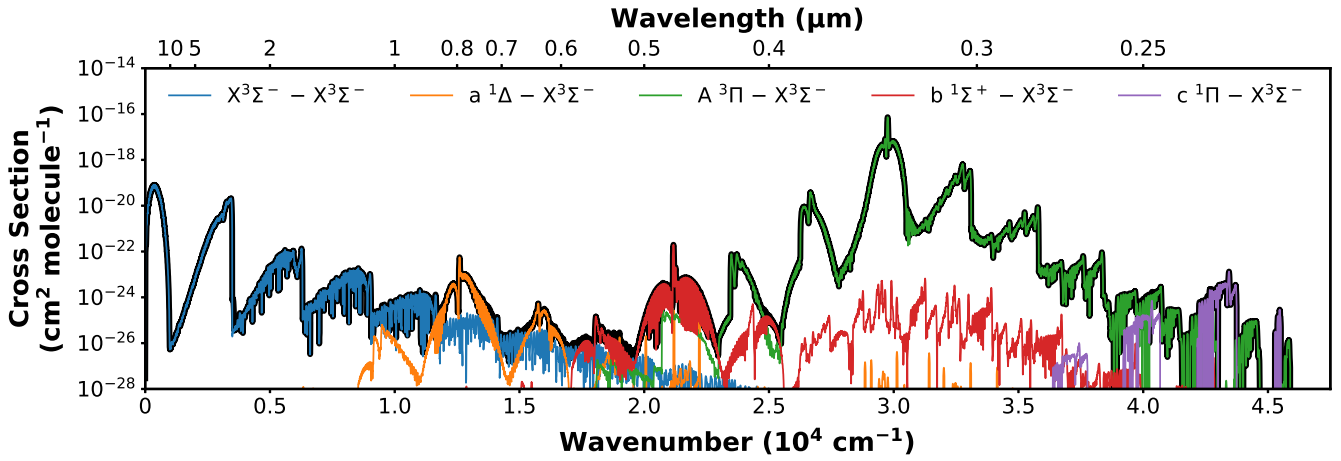


**Figure 5.** The total  $^{14}\text{N}^1\text{H}$  absorption cross section decomposed for 0 – 47,500  $\text{cm}^{-1}$  at 2,000 K.

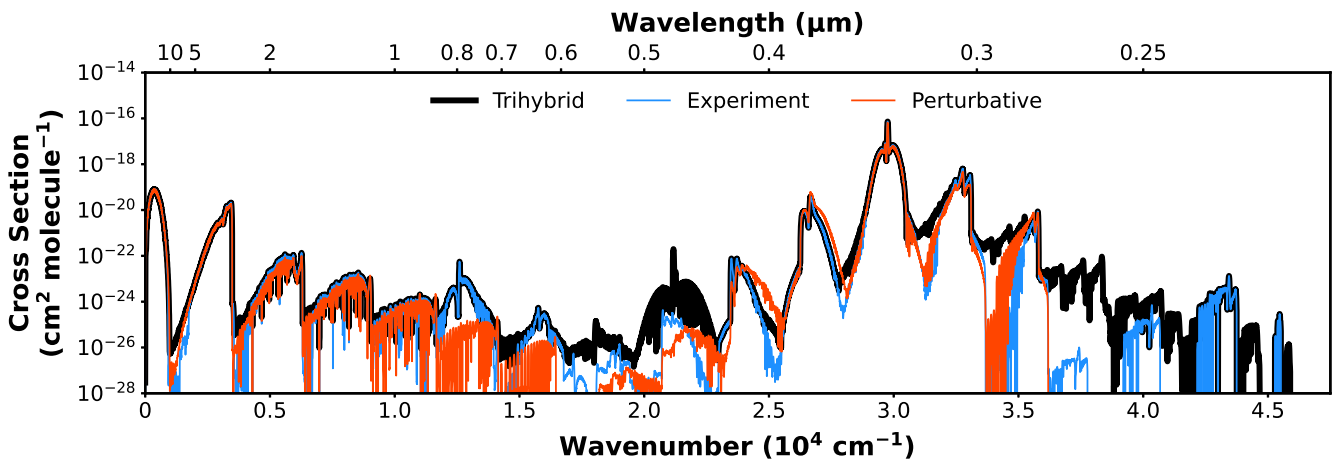


**Figure 6.** The total  $^{14}\text{N}^1\text{H}$  absorption cross section simulated at 2,000 K from different sources. The black, blue and orange cross sections show transitions accounted for by the κNIGHT trihybrid line list, MARVEL experimental line list by Darby-Lewis et. al. (2019) (with variational intensities) and MoLLIST perturbative line list by Brooke et. al. (2014,2015); Fernando et. al. (2018), respectively.

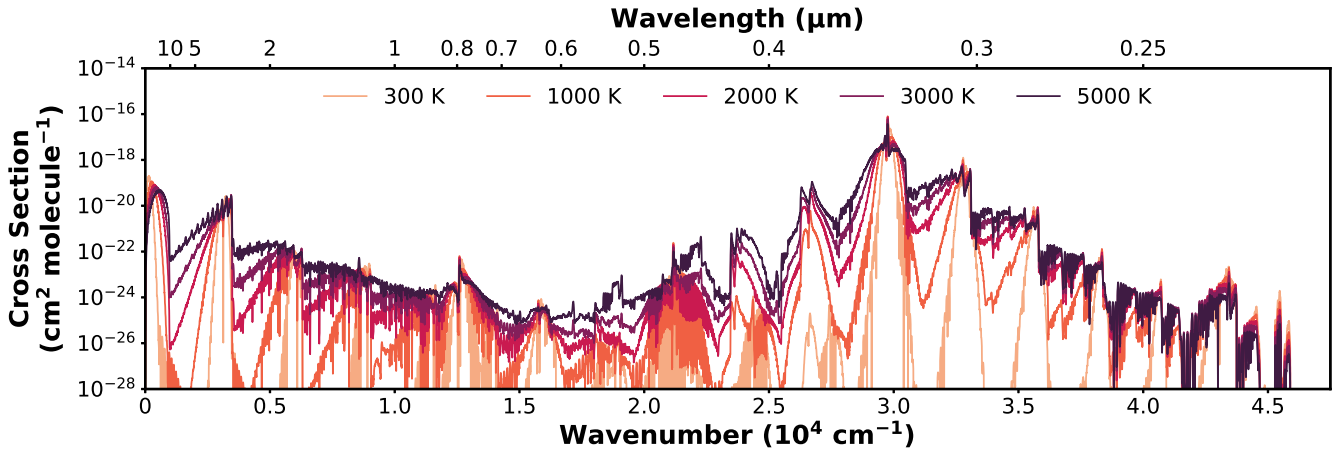


Figure 7. The total  $^{14}\text{N}^1\text{H}$  absorption cross section simulated at several temperatures.

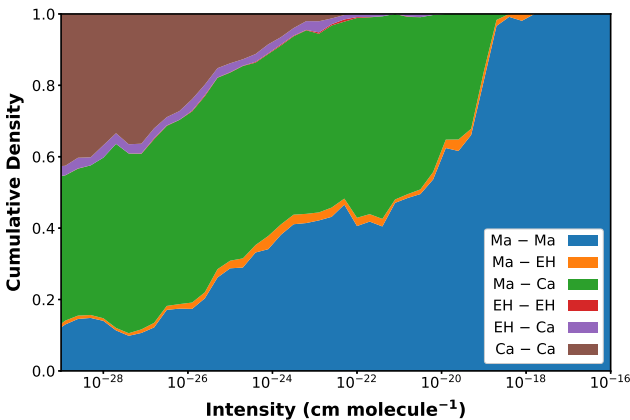


Figure 8. The cumulative density of energy sources as a function of transition intensity at 2,000 K. The abbreviations Ma, EH and Ca represent the experimental (MARVEL), perturbative (effective Hamiltonian) and variational (calculated) methodologies, respectively.

#### 5.4 Discussion and future direction

For the anticipated applications of NH spectral data in all regions except the far-IR, the  $\kappa\text{NIGHT}$  line list should provide information of sufficient quality. It should not be used for high-accuracy studies in the far-IR region (*i.e.* the rotational spectroscopy) because, in this spectral region, there is significant hyperfine structure that are not incorporated in this spectroscopic model and thus not present in this line list. Specifically, hyperfine interactions are due to the nuclear spins of  $^{14}\text{N}$  ( $I = 1$ ) and  $^1\text{H}$  ( $I = 1/2$ ) for  $^{14}\text{N}^1\text{H}$ . This hyperfine structure is resolved in most rotational studies, but not for any of the higher wavenumber studies (Darby-Lewis et al. 2019). With this limitation in experimental data, at this stage, the best line list data source for modelling the rotational (far-IR) spectroscopy of  $^{14}\text{N}^1\text{H}$  remains distinct from the best line list data source of the infrared-UV absorption ( $\kappa\text{NIGHT}$ , developed here). For the far IR observations, it is recommended that astronomers use line list data from Splatalogue (Remijan et al. 2007), which combines both JPL (Pickett et al. 1998) and CDMS

(Endres et al. 2016) data for NH in one convenient online interface. It should be noted that an extended version of Duo has just been released (Qu et al. 2022) that does allow hyperfine-resolved line lists to be generated (although for only one nucleus with nuclear spin); this could be a future avenue for the improvement of NH data and could potentially allow a unified single source of spectroscopic data across the electromagnetic spectrum.

Any improvements in the accuracy of the existing non-hyperfine-resolved line list should focus on more precise quantification of the parameters relevant to forbidden transitions in the visible spectral region. This can be accomplished by improvements in understanding the energies of the  $b^1\Sigma^+$  state (*e.g.* from high-resolution spectroscopy experiments) and the  $a^1\Delta - A^3\Pi$  and  $b^1\Sigma^+ - A^3\Pi$  spin-orbit couplings (theoretical models may actually be a better approach here to avoid complications from other factors). The current  $\kappa\text{NIGHT}$  trihybrid line list demonstrates that these spin-orbit coupling terms are the physical cause of the strongest transitions in the spectral region from 450 – 800 nm, the spin-forbidden  $a^1\Delta - X^3\Sigma^-$  and  $b^1\Sigma^+ - X^3\Sigma^-$  transitions. The current model should have semi-quantitative accuracy as the reliability of *ab initio* calculations for NH are high. That said, experimental verification would be welcome.

## 6 CONCLUSIONS

The best current understanding of NH spectroscopy across the infrared to UV regions is presented herein through the novel  $\kappa\text{NIGHT}$  trihybrid line list, which was produced from a new spectroscopic model containing five low-lying electronic states  $X^3\Sigma^-$ ,  $A^3\Pi$ ,  $a^1\Delta$ ,  $b^1\Sigma^+$  and  $c^1\Pi$  for all major isotopologues ( $^{14}\text{N}^1\text{H}$ ,  $^{14}\text{N}^2\text{H}$ ,  $^{15}\text{N}^1\text{H}$  and  $^{15}\text{N}^2\text{H}$ ). In order to ensure the highest accuracy of line positions currently possible, experimental (MARVEL; Darby-Lewis et al. (2019)) and perturbative (MoLLIST; Brooke et al. (2014, 2015); Fernando et al. (2018)) energies have been incorporated into both the spectroscopic model fitting procedure and the final trihybrid line list. In order to ensure very high completeness, novel *ab initio* data were utilised to create a full variational spectroscopic model. It should be cautioned that the Splatalogue data (Remijan et al. 2007) for

NH are preferable for far-IR studies where available, given that these data are hyperfine resolved. The resulting hyperfine line splittings are important for the accurate modelling of rotational spectral lines (observed in far-IR studies), although these have thus far not been resolved in the mid-IR to UV spectral regions.

The strong NH absorption lines are unfortunately in inconvenient spectral ranges for ground-based telescopes (UV peaking at 335 nm, mid-IR near water absorption and far-IR), and thus molecular detection via high-resolution cross-correlation techniques will likely be very challenging. Nevertheless, the molecular data for NH is sufficient to allow these investigations from 280 – 440 nm and above 667 nm. Space-based telescopes are thus the preferred way of detecting NH in astronomical environments and the new κNIGHT line list will support astronomers in identifying NH and quantifying its abundance using telescopes across a variety of spectral regions, including UV, visible, near and mid-IR.

## ACKNOWLEDGEMENTS

This research was undertaken with the assistance of resources from the National Computational Infrastructure (NCI Australia), an NCRIS enabled capability supported by the Australian Government.

The authors declare no conflicts of interest.

The authors thank Charlie Drury, Sergey Yurchenko and Jonathan Tennyson for sharing their insights into the astronomical importance of NH.

## DATA AVAILABILITY

The most up-to-date κNIGHT line list data for NH are available on the ExoMol website ([www.exomol.com](http://www.exomol.com)), specifically:

- The main κNIGHT .model file (14N1H\_kNigHt.model).
- The main κNIGHT partition function from 0 – 10,000 K (14N1H\_kNigHt.pf).
- The main κNIGHT .states file (14N1H\_kNigHt.states).
- The main κNIGHT .trans file (14N1H\_kNigHt.trans).
- All other isotopologue .model, .pf, .states and .trans files (in their respective folders).

These data at the time of publication are also available as supporting information for this paper. The Molpro quantum chemistry input files for the MRCI calculations are also included to assist data reproducibility.

## REFERENCES

Amiot C., Dulieu O., Vergès J., 1999, *Phys. Rev. Lett.*, 83, 2316  
 Aoki W., Tsuji T., 1997, *A&A*, 328, 175  
 Babcock H. D., 1945, *ApJ*, 102, 154  
 Barklem P. S., Collet R., 2016, *Astronomy and Astrophysics*, 588  
 Bernath P. F., Amano T., 1982, *Journal of Molecular Spectroscopy*, 95, 359  
 Bhasi P., Nhlabatsi Z. P., Sitha S., 2015, *Phys. Chem. Chem. Phys.*, 17, 32455  
 Boudjaadar D., Brion J., Chollet P., Guelachvilli G., Vervloet M., 1986, *Journal of Molecular Spectroscopy*, 119, 352  
 Brackmann C., Nilsson E. J., Nauclér J. D., Aldén M., Konnov A. A., 2018, *Combustion and Flame*, 194, 278

Brady R. P., Yurchenko S. N., Tennyson J., Kim G.-S., 2023, *Monthly Notices of the Royal Astronomical Society*, 527, 6675  
 Brazier C. R., Ram R. S., Bernath P. F., 1986, *Journal of Molecular Spectroscopy*, 120, 381  
 Brooke J. S. A., Bernath P. F., Western C. M., van Hemert M. C., Groenenboom G. C., 2014, *The Journal of Chemical Physics*, 141, 054310  
 Brooke J. S. A., Bernath P. F., Western C. M., 2015, *The Journal of Chemical Physics*, 143, 026101  
 Brown J. M., Carrington A., 2003, *Rotational Spectroscopy of Diatomic Molecules*  
 Campbell W. C., Tsikata E., Lu H. I., Van Buuren L. D., Doyle J. M., 2007, *Physical Review Letters*, 98  
 Cernicharo J., Goicoechea J. R., Caux E., 2000, *The Astrophysical Journal*, 534, L199  
 Civiš S., Pastorek A., Ferus M., Yurchenko S. N., Boudjema N.-I., 2023, *Molecules*, 28  
 Crawford I. A., Williams D. A., 1997, *Monthly Notices of the Royal Astronomical Society*, 291, L53  
 Darby-Lewis D., et al., 2019, *Journal of Molecular Spectroscopy*, 362, 69  
 Endres C. P., Schlemmer S., Schilke P., Stutzki J., Müller H. S., 2016, *Journal of Molecular Spectroscopy*, 327, 95  
 Fernando A. M., Bernath P. F., Hodges J. N., Masseron T., 2018, *Journal of Quantitative Spectroscopy and Radiative Transfer*, 217, 29  
 Flores-Mijangos J., Brown J. M., Matsushima F., Odashima H., Takagi K., Zink L. R., Evenson K. M., 2004, *Journal of Molecular Spectroscopy*, 225, 189  
 Furtenbacher T., Császár A. G., Tennyson J., 2007, *Journal of Molecular Spectroscopy*, 245, 115  
 Geller M., Farmer C. B., Norton R. H., Sauval A. J., Grevesse N., 1991, *A&A*, 249, 550  
 Glarborg P., Miller J. A., Ruscic B., Klippenstein S. J., 2018, *Progress in Energy and Combustion Science*, 67, 31  
 Grevesse N., Lambert D. L., Sauval A. J., van Dishoeck E. F., Farmer C. B., Norton R. H., 1990, *A&A*, 232, 225  
 Gupta V., Tandon P., Mishra P., 2013, *Advances in Space Research*, 51, 797  
 Hack W., Mill T., 1990, *Journal of Molecular Spectroscopy*, 144, 358  
 Hall J. L., Adams H., Kasper J. V. V., Curl R. F., Tittel F. K., 1985, *J. Opt. Soc. Am. B*, 2, 781  
 Hamdan A., Liu J. L., Cha M. S., 2018, *Plasma Chemistry and Plasma Processing*, 38, 1003  
 Harilal S., Brumfield B. E., Phillips M. C., 2018, *Physics of Plasmas*, 25  
 Henderson R. D. E., Shayesteh A., Tao J., Haugen C. C., Bernath P. F., Le Roy R. J., 2013, *The Journal of Physical Chemistry A*, 117, 13373  
 Hikida T., Maruyama Y., Saito Y., Mori Y., 1988, *Chemical Physics*, 121, 63  
 Huber K. P., Herzberg G., 1979, *Molecular Spectra And Molecular Structure, IV. Constants Of Diatomic Molecules*  
 J.-M. Flaud C. C.-P., Maillard J., 1976, *Molecular Physics*, 32, 499  
 Klaus T., Takano S., Winnewisser G., 1997, *A&A*, 322, L1  
 Lambert D. L., Brown J. A., Hinkle K. H., Johnson H. R., 1984, *ApJ*, 284, 223  
 Lamoureux N., Gasnot L., Desgroux P., 2019, *Proceedings of the Combustion Institute*, 37, 1313  
 Le Roy R. J., 1999, *Journal of Molecular Spectroscopy*, 194, 189  
 Le Roy R. J., 2017, *Journal of Quantitative Spectroscopy and Radiative Transfer*, 186, 167  
 Le Roy R. J., Huang Y., 2002, *Journal of Molecular Structure: THEOCHEM*, 591, 175

- Leopold K. R., Evenson K. M., Brown J. M., 1986, [The Journal of Chemical Physics](#), 85, 324
- Letelier J., Senent M., 2006, [Spectrochimica Acta Part A: Molecular and Biomolecular Spectroscopy](#), 65, 1030
- Lewen F., Brünken S., Winnewisser G., Šimečková M., Štěpán Urban 2004, [Journal of Molecular Spectroscopy](#), 226, 113
- Li D., Bian W., 2021, [Frontiers in Chemistry](#), 9, 1
- Liu X., Truppe S., Meijer G., Pérez-Ríos J., 2020, [Journal of Cheminformatics](#), 12
- Mann A. P. C., Williams D. A., 1984, [Monthly Notices of the Royal Astronomical Society](#), 209, 33
- Mashruk S., Alnasif A., Yu C., Thatcher J., Rudman J., Peronski L., Meng-Choung C., Valera-Medina A., 2023, [Journal of Ammonia Energy](#), 1, 21
- McGuire B. A., 2022, [The Astrophysical Journal Supplement Series](#), 259, 30
- McKemmish L. K., 2021, [WIREs Computational Molecular Science](#), 11
- Melosso M., Bizzocchi L., Tamassia F., Degli Esposti C., Canè E., Dore L., 2019, [Phys. Chem. Chem. Phys.](#), 21, 3564
- Meyer D. M., Roth K. C., 1991, [ApJ](#), 376, L49
- Owono Owono L. C., Jaidane N., Kwato Njock M. G., Ben Lakhdar Z., 2007, [Journal of Chemical Physics](#), 126
- Perri A. N., Taher F., McKemmish L. K., 2023, [Monthly Notices of the Royal Astronomical Society](#), 524, 4631
- Persson, C. M. et al., 2010, [A&A](#), 521, L45
- Persson, C. M. et al., 2012, [A&A](#), 543, A145
- Pflieder R., Ouerhani T., Belmonte T., Nikitenko S. I., 2017, [Phys. Chem. Chem. Phys.](#), 19, 26272
- Pickett H., Poynter R., Cohen E., Delitsky M., Pearson J., Müller H., 1998, [Journal of Quantitative Spectroscopy and Radiative Transfer](#), 60, 883
- Plomp V., Gao Z., Cremers T., van de Meerakker S. Y. T., 2019, [Phys. Rev. A](#), 99, 033417
- Polyansky O. L., Kyuberis A. A., Lodi L., Tennyson J., Yurchenko S. N., Ovsyannikov R. I., Zobov N. F., 2017, [Monthly Notices of the Royal Astronomical Society](#), 466, 1363
- Qu Q., Yurchenko S. N., Tennyson J., 2022, [Journal of Chemical Theory and Computation](#), 18, 1808
- Ram R. S., Bernath P. F., 1986, [J. Opt. Soc. Am. B](#), 3, 1170
- Ram R. S., Bernath P. F., 2010, [Journal of Molecular Spectroscopy](#), 260, 115
- Ram R. S., Bernath P. F., Hinkle K. H., 1999, [The Journal of Chemical Physics](#), 110, 5557
- Ramsay D. A., Sarre P. J., 1982, [Journal of Molecular Spectroscopy](#), 93, 445
- Remijan A. J., Markwick-Kemper A., ALMA Working Group on Spectral Line Frequencies 2007, in [American Astronomical Society Meeting Abstracts](#). p. 132.11
- Roy M., Tyuterev V. G., 2007, [Phys. Chem. Chem. Phys.](#), 9, 2538
- Robinson A., Brown J., Jesus Flores-Mijangos L. Z., Jackson M., 2007, [Molecular Physics](#), 105, 639
- Smith V. V., Lambert D. L., 1986, [ApJ](#), 311, 843
- Snedden C., 1973, [ApJ](#), 184, 839
- Song Z., Shi D., Sun J., Zhu Z., 2016, [Computational and Theoretical Chemistry](#), 1093, 81
- Swings P., Elvey C. T., Babcock H. W., 1941, [ApJ](#), 94, 320
- Syme A.-M., McKemmish L. K., 2021, [Monthly Notices of the Royal Astronomical Society](#), 505, 4383
- Szabó P., Gustafsson M., 2019, [MNRAS](#), 483, 3574
- Tennyson J., Yurchenko S. N., 2012, [Monthly Notices of the Royal Astronomical Society](#), 425, 21
- Tennyson J., et al., 2020, [Journal of Quantitative Spectroscopy and Radiative Transfer](#), 255
- Ubachs W., Meyer G., ter Meulen J. J., Dymanus A., 1986, [Journal of Molecular Spectroscopy](#), 115, 88
- Villanueva G. L., Smith M. D., Protopapa S., Faggi S., Mandell A. M., 2018, [Journal of Quantitative Spectroscopy and Radiative Transfer](#), 217, 86
- Wagenblast R., Williams D. A., Millar T. J., Nejad L. A. M., 1993, [Monthly Notices of the Royal Astronomical Society](#), 260, 420
- Werner H. J., et al., 2020, [Journal of Chemical Physics](#), 152
- Weselak T., Galazutdinov G. A., Beletsky Y., Krelowski J., 2009, [Monthly Notices of the Royal Astronomical Society](#), 400, 392
- Western C. M., 2017, [Journal of Quantitative Spectroscopy and Radiative Transfer](#), 186, 221
- Yan N.-Z., Yang C.-L., Sun Z.-P., Wang M.-S., Ma X.-G., 2021, [Spectrochimica Acta Part A: Molecular and Biomolecular Spectroscopy](#), 250, 119229
- Yarkony D. R., 1989, [The Journal of Chemical Physics](#), 91, 4745
- Yurchenko S. N., Lodi L., Tennyson J., Stolyarov A. V., 2016, [Computer Physics Communications](#), 202, 262
- Yurchenko S. N., Al-Refaie A. F., Tennyson J., 2018, [Astronomy & Astrophysics](#), 614, A131
- van de Meerakker S. Y. T., Sartakov B. G., Mosk A. P., Jongma R. T., Meijer G., 2003, [Phys. Rev. A](#), 68, 032508
- van de Meerakker S. Y. T., Labazan I., Hoekstra S., Küpper J., Meijer G., 2006, [Journal of Physics B: Atomic, Molecular and Optical Physics](#), 39, S1077
- van den Heuvel F., Meerts W., Dymanus A., 1982, [Chemical Physics Letters](#), 92, 215
- zhi Jin B., Deng Y.-F., xiu Li G., meng Li H., 2022, [International Journal of Hydrogen Energy](#), 47, 36046